Geologica Acta, Vol.15, Nº 3, September 2017, 217-230, I-III
DOI: 10.1344/GeologicaActa2017.15.3.5

geologica acta

Multi proxy approach to evaluate and delineate the potential of hot springs in the Kotli District (Kashmir, Pakistan)

M. ANEES[1,2] M.M. SHAH[1,3*] A.A. QURESHI[4] S. MANZOOR[4]

[1]Department of Earth Sciences, Quaid-i-Azam University
45320 Islamabad, Pakistan. Anees E-mail: muhammad.anees.pk@gmail.com
Shah E-mail: mshah@qau.edu.pk

[2]Pakistan Space and Upper Atmosphere Research Commission (SUPARCO)
75270, Pakistan

[3]SE-Asia Carbonate Research Laboratory (SEACaRL) Universiti Teknologi PETRONASCO)
32610 Seri Iskandar, Malaysia

[4]Radiation Physics Lab, Physics Department, COMSATS Institute of Information Technology
Islamabad, Pakistan. Qureshi E-mail: aziz_qureshi@comsats.edu.pk
Manzoor E-mail: smanzoor@comsats.edu.pk

*Corresponding author

ABSTRACT

Tattapani hot springs are located near the Kotli District of Azad Kashmir, Pakistan. This study evaluates these hot springs based on surface geological information, radon emission measurements, hydro-geochemical and isotopic signatures and potential source mechanisms. Field observations reveal that the hot springs are located at the crest of the Tattapani anticline along the faulted contact of Cambrian carbonates with Paleocene siliciclastics. In addition, remnants of igneous intrusions in the Cambrian carbonates are commonly observed. Spatial distribution of radon emissions (ranging between 2.1 and 29.5KBq m^{-3}) indicates an anomalous zone located over the Cambrian-Paleocene faulted contact. Hydro-geochemical data show sodium-bicarbonate affinity of hot springs. The highest surface temperature of these springs is recorded at 60.8ºC. Average reservoir temperatures based on silica and cation geo-thermometers are 101ºC and 115ºC, respectively. Giggenbach ternary diagram (Na-K-Mg) suggests a non-equilibrium state between fluid and rock, whereas isotopic and chemical data indicate heat loss by conductive cooling and mixing with groundwater during the flow of thermal water up to the surface. Oxygen and deuterium isotopes indicate that thermal water is of meteoric origin, rain and/or snow in the north at higher altitudes providing the potential recharge. Furthermore, absence of tritium in the thermal water suggests a residence time of more than 50 years.

KEYWORDS | **Hot springs. Radon survey. Hydro-geochemistry. Geo-thermometry. Isotope composition. Geothermal system.**

INTRODUCTION

Renewable energies are an environment friendly alternative to the conventional energy resources such as fossil fuel. Geothermal energy is one of the key components in the chain of renewable energy resources that is not only eco-friendly, but cheap as compared to other renewable resources. The exploitation of geothermal energy resources can help in the production of clean energy without any significant environmental and climatic impact (Lund *et al.*, 2005). Hot

springs, with their substantial flow rates and varying temperatures (mild warm to boiling water), offer an ideal platform for exploitation of geothermal energy. Hot springs can be used as a cheap and easy source for power generation and/or domestic uses at local level.

In Pakistan, geothermal energy sources are mostly concentrated along the boundaries of the Indian and Eurasian plate or along other active seismic zones. The junction between the two tectonic plates forms part of northern Pakistan, which makes it favourable for presence of exploitable sources of geothermal energy (Fig. 1A). The collision between the Indian and Eurasian plates has triggered the geothermal activity in the region along with the activation of E-W trending regional thrust systems, *e.g.* Main Mantle Thrust, Main Karakoram Thrust and Main Boundary Thrust (Bakht, 2000; Zaigham *et al.*, 2009). Studies have been conducted over several decades to evaluate the potential of hot springs found mainly in the northern parts of the country (Shuja, 1986). These studies have primarily focused on the chemical composition and the regional geological setting of hot springs (Todaka *et al.*, 1988). Other investigations have dealt with the evolution, origin, age, water/rock interactions and reservoir temperatures of the hot springs (Ahmad *et al.*, 2000; 2001; 2002).

The present study deals with the geochemical properties and radon emissions of Tattapani hot springs, located near Kotli city, Azad Kashmir, Pakistan. Previous studies focused on lithostratigraphic and structural context, biodiversity and paleoenvironmental conditions in the study area (Ashraf *et al.*, 1986; Wells and Gingerich, 1987; Munir and Baig, 2006; Aadil and Rehman, 2013). The main objective of this study is to understand the chemical nature and origin of Tattapani hot springs and their relationship with their geological settings. Within this context, this paper presents the hydro-geochemical and isotopic characterization of the thermal water with emphasis on: i) thermal reservoir temperature, based on chemical geo-thermometry; ii) origin and residence time, based on isotopic study; iii) zones of anomalous radon emission and iv) subsurface hydrological processes.

Study area and geological setting

The study area is located in the vicinity of the town of Tattapani in Azad Kashmir, Pakistan (Fig. 1B). The Tattapani hot springs are located 26km north of Kotli city and 150km east of Islamabad (Fig. 1B), emerging from the gravely bank of Poonch River and discharging directly into the river. Surface manifestations comprise numerous springs (dependent upon local seasonal variations) which emerge at two sites, the primary one at the northern bank of Poonch River (6-springs) and the secondary site at the southern bank (2-springs) of the river (Fig. 2).

Kotli area lies on the SE of the Hazara-Kashmir Syntaxis (HKS) and is considered to be part of sub to lower Himalayas (Fig. 1B). The Main Boundary Thrust (MBT), trending in a NW-SE direction, has been demarcated by Wadia (1928) passing just South of the Kotli city (Fig. 1B). The two prominent structural features of the area are the Tattapani-Karela and the Palana-Divigarh plunging anticlines (Fig. 1C). These major folds are trending NW-SE and have fold axis parallel to that of the Pir Panjal Range (Wadia, 1928). Overall, the direction of compressive forces in the area seems to be NE-SW. Tattapani-Karela anticline is approx. 28km long and 4.5km wide with NW-SE trending axis with 15º–30º plunge (Fig.1C). The dolomitized stromatolitic limestone of the Muzaffarabad Formation (Cambrian) comprises the bulk of the anticline. In the study area, the Riasi Thrust, a part of the MBT (trending NW-SE), is located towards the southeast, marking a faulted contact between the Murree Formation and the Miocene to Pleistocene Middle Siwalik Group (Hussain *et al.*, 2009; Thakur *et al.*, 2010; Aadil and Rehman, 2013).

The Tattapani hot springs are located over the NW-SE trending Tattapani anticline. Stratigraphy of the area comprises from Cambrian to recent carbonate and clastic successions. The Muzaffarabad Formation, mostly composed of stromatolitic limestone and dolostone, is exposed in the core of the anticline, and is overlain unconformably by the shales of the Palaeocene Patala Formation (Fig. 1C). It is noteworthy that an Eocene succession (*i.e.* Margalla Hill Limestone, Chorgali and Kuldana formations), not mapped by the Geological Survey of Pakistan (Fig. 1C), has been observed on both flanks of the Tattapani anticline. However, the contact between the Palaeocene and Eocene rocks was not clear. The Murree Formation (Miocene), composed of maroonish sandstone along with siltstone and mudstone, overlays older rocks and is exposed in regions around the flanks of anticline. A magmatic intrusion (possibly post-Eocene) was observed along the carbonate succession near the secondary hot spring site (Fig. 2). The intrusive body was sandwiched between the quartzite member of the Muzaffarabad Formation and the shales of the Patala Formation. The intrusive rock is medium to coarse grained and dark bluish grey to greenish grey. The weathering colour is yellowish to light grey. Rocks were mostly altered by thermal fluids. Similar intrusive bodies were reported towards the SE along the northern flank of Tattapani anticline (Ashraf *et al.*, 1983).

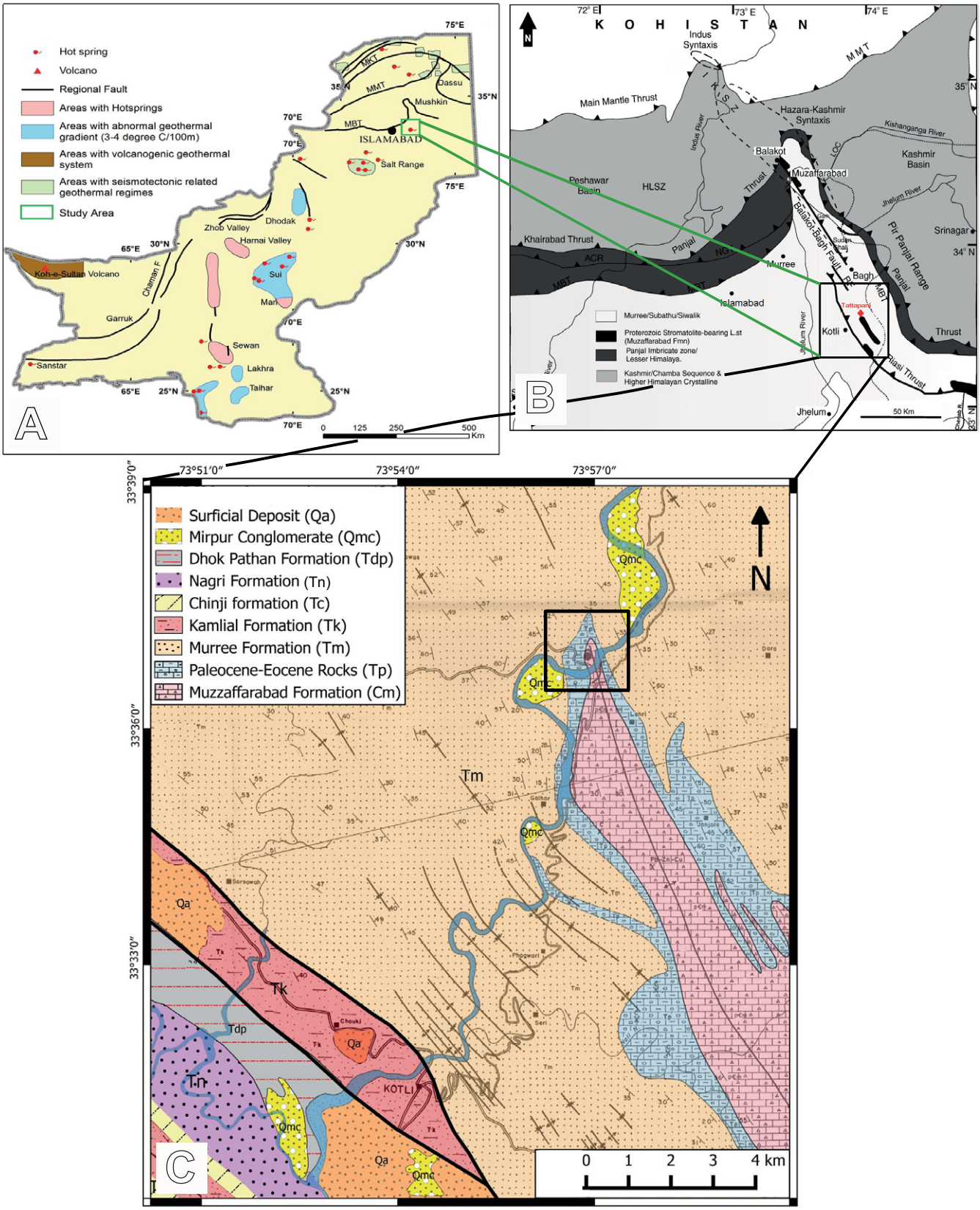

FIGURE 1. A) Map showing the geothermal manifestations in Pakistan along with major faults (after Zaigham *et al.*, 2009). B) Tectonic map of North Pakistan showing location of study area along with major tectonic thrusts (Thakur *et al.*, 2010); RF: Rawalkot Fault; IKSZ: Indus Kohistan Seismic Zone; HLSZ: Hazara Lower Seismic Zone; NGT: Nathia Gali Thrust, MBT: Main Boundary. C) Geological map of Kotli district (after Mureed *et al.*, 2004), black square shows sampling area.

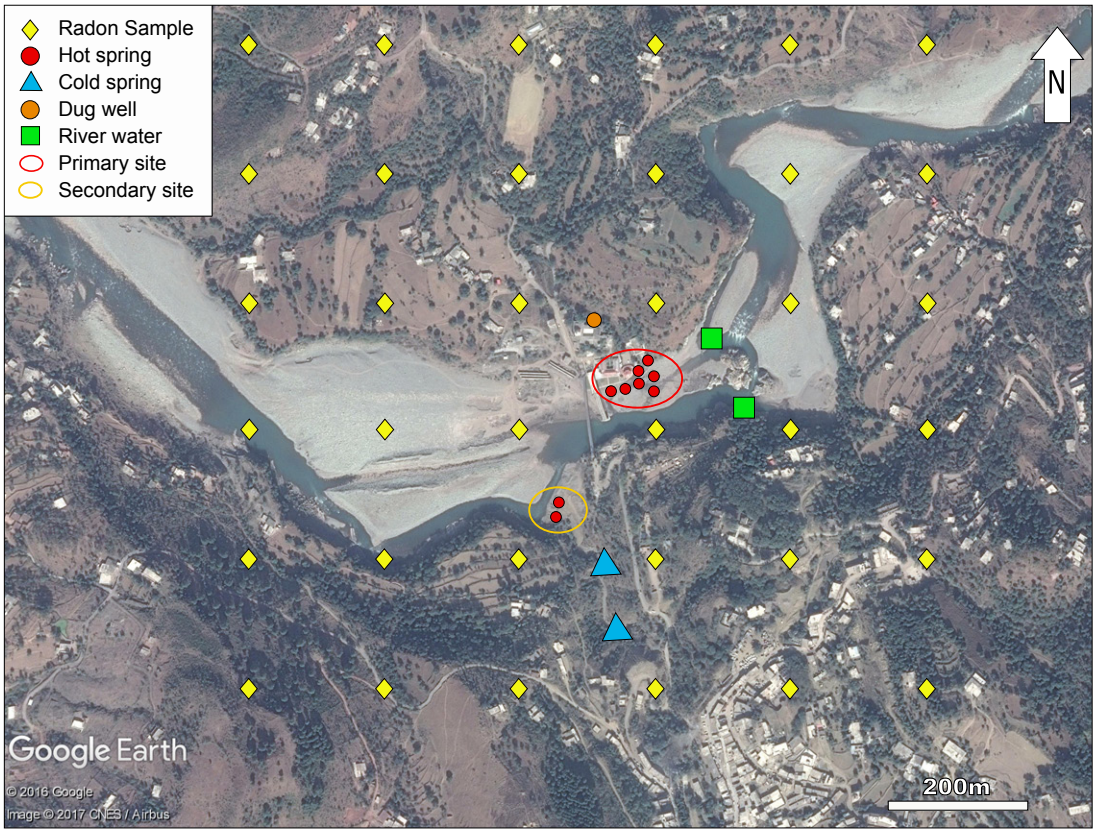

FIGURE 2. Satellite-view image showing radon sampling points (yellow diamond symbols) in the sampling grid along with location of samples collected from the thermal and fresh water sites in the study area.

METHODOLOGY

Radon measurement

A radon survey was selected to detect the presence of permeable zones (faults and fractures) in the geothermal field (Gingrich, 1984), that may act as pathways for fluid movement in the study area. This methodology has been adopted for geothermal exploration in many countries such as New Zealand (Whitehead, 1984), USA (Fleischer, 1988), Mexico (Lopez *et al.*, 1987; Balcazar *et al.*, 1993), and Indonesia (Phuong *et al.*, 2012; Haerudin *et al.*, 2013). A comprehensive methodology was adopted to carry out radon measurements in soil and water.

For soil-gas radon measurements, a sampling grid covering an area of 1km^2 was designed and plotted around the hot springs (Fig. 2). In total, 36 equally spacing (200m) sampling points were contemplated to fulfil the purposes of sampling. RAD-7 Electronic Radon Detector (DURRIDGE Co., USA) was used for the measurement of radon concentration in the Tattapani area. A stainless soil-gas probe was used for in-soil radon measurement. Alpha particle emission activity in the soil-air sample was recorded using RAD-7. Air was pumped into the instrument and allowed to circulate for 20min to record the alpha particle emission measurement. Measurement for radon in water was made on-site for samples collected from an open well, hot springs and cold springs. The RAD H_2O technique of RAD-7 was used to calculate the concentration of radon levels in water samples. This took about 30min.

Pre-set grab samples from RAD-7 were taken in single runs with four cycles of 5min each. Mean radon concentration was calculated averaging the radon concentration measured in all four cycles using the following equation

$$222Rn(KBq/m^3) = \frac{C1 + C2 + C3 + C4}{4} \quad (1)$$

where C1, C2, C3 and C4 are the radon concentrations of the respective cycles.

Chemical and isotopic analysis of water

For the chemical and isotope analysis, eight hot springs were selected along with water samples from the nearby river, dug well and fresh water springs. Water samples were

collected in high quality Polyethylene (PET) plastic bottles: 200ml for cations, anions, silica (SiO_2), and isotopes (^2H, ^{18}O), and 1L for ^3H. Samples collected for cation analysis were acidified with 1% HNO_3 (yielding pH<2) to avoid precipitation upon storage. Samples collected for SiO_2 were diluted (1:1) with deionized water to prevent silica polymerization (Arnórsson, 2000). Samples of river water were filtered using filter paper (0.45µm).

Physico-chemical parameters such as temperature, pH, flow rate, Total Dissolved Solid (TDS) and Electrical Conductivity (EC) were determined in the field. Temperature and pH measurements were made using Crison pH-meter PH25+, which was calibrated by using three buffer solutions of pH 4.00, pH 7.00 and pH 9.00. Electrode was placed into the water sample and left until thermal equilibrium was established. Readings were recorded up to 0.01 pH-units together with the temperature of the water. For EC and TDS, a multimeter was used. Electrode was washed with deionized water before and after the measurement to ensure the precision.

Chemical analyses were carried out through Atomic Absorption Spectrometry (AAS) using a Varian Flame Atomic Absorption Spectrometer. A direct read out is given for concentrations of Na, K, Ca and Mg (Giggenbach and Goguel, 1988) in mg/l. Concentration of silica (dissolved Si in water) was measured using a UV–visible spectrophotometry. For concentrations of major anions (*e.g.* HCO_3, Cl and SO_4), the water samples were analysed using the methods described by APHA (2005) and Watson (1978).

The stable isotope compositions (^2H and ^{18}O) in water samples were measured by mass spectrometry. Using the CO_2 equilibration method (Epstein and Mayeda, 1953), ^{18}O values of water were analysed relative to V-SMOW with a standard error of ±0.1‰. The tritium content of the samples was determined by liquid scintillation counting after electrolytic enrichment of the water samples with a standard error of ±1TU (Hussain and Asghar, 1982).

RESULTS AND DISCUSSION

Radon emissions

Out of 36 radon sampling locations, 6 points were located over the loose gravel (fluvial), 7 on the shaley rocks, 7 on the sandstone of the Murree Formation, 4 on the carbonates of the Muzaffarabad Formation and 12 on the thick soil covering the underlying rocks (Table I). Radon concentration varied between 2.1 and 29.5KBqm^{-3} with a mean value of 7.62KBqm^{-3} and standard deviation of 6.23KBqm^{-3} (Table I). Concentration of radon was highest at sampling point A3 and lowest at C5. Sampling points A3, B3, F3, and F4 showed high anomalous values relative to those of other locations. Variations in radon emission from different rocks and soils depend upon the permeability and structural components (faults / fractures) along with various climatic aspects (Mogro-Campero and Fleischer, 1977). Studies conducted worldwide have revealed a persistent low radon level emission from Earth's crust to atmosphere except for sites of geological fault, uranium deposits, volcanoes and geothermal sources (Nishimura and Katsura, 1990). In the present study, the radon concentration was relatively low at sample points located on or near the river bank. Gravel deposited along the river bank was not consolidated, so the large interconnected pore spaces between the sediments possibly provide pathways for surface air to dilute the gases escaping from the subsurface (Table I).

Soil gas radon data have been statistically distributed into three populations: low (less than 6.23KBqm^{-3}), high (between 6.23 and 13.84KBqm^{-3}) and anomalous concentrations (between 13.84 and 21.46KBqm^{-3}; Table I). Spatially, two zones with anomalous radon concentrations were identified quite opposite to each other on the contour map, *i.e.* one in the South and the other in the North (Fig. 3). However, a N-S trending zone can be assumed if both anomalies are joined together. The N-S trending zone with high and anomalous radon concentrations happened to be located just above the contact between the Muzaffarabad and Patala formations where an igneous intrusion was observed near the secondary site (Fig. 4). Generally, the process of out-gassing through crust is a fracture controlled phenomenon, which varies according to the fracture spatial distribution (Sac *et al.*, 2011). Once released from source, radon tends to migrate upwards. The movement of radon and its concentration in soil is influenced by a number of factors including the permeability of rocks, porosity and humidity, atmospheric pressure, micro-cracks, surface winds and granulations (Toutain and Baubron, 1999). A possible interpretation for these anomalous zones in the study area could be related to the presence of pathways along the contact allow that the movement of fluids from depth to surface.

Data from six traverse lines of the grid (A, B, C, D, E and F) that run across the Tattapani anticline was plotted to evaluate the effect of lithological changes over radon concentration as shown in Figure 4. Radon releasing capacity of rocks and soil (Morawska and Phillips, 1993), host rock permeability and flow of carrier gases (CO_2, CH_4, N_2 and He) were found to be the influencing factors for in-soil radon concentration, analysed at surface conditions (Ball *et al.*, 1991). The increase in radon concentration is associated with the escape of soluble radon from water at high temperatures. The shales of the Patala Formation

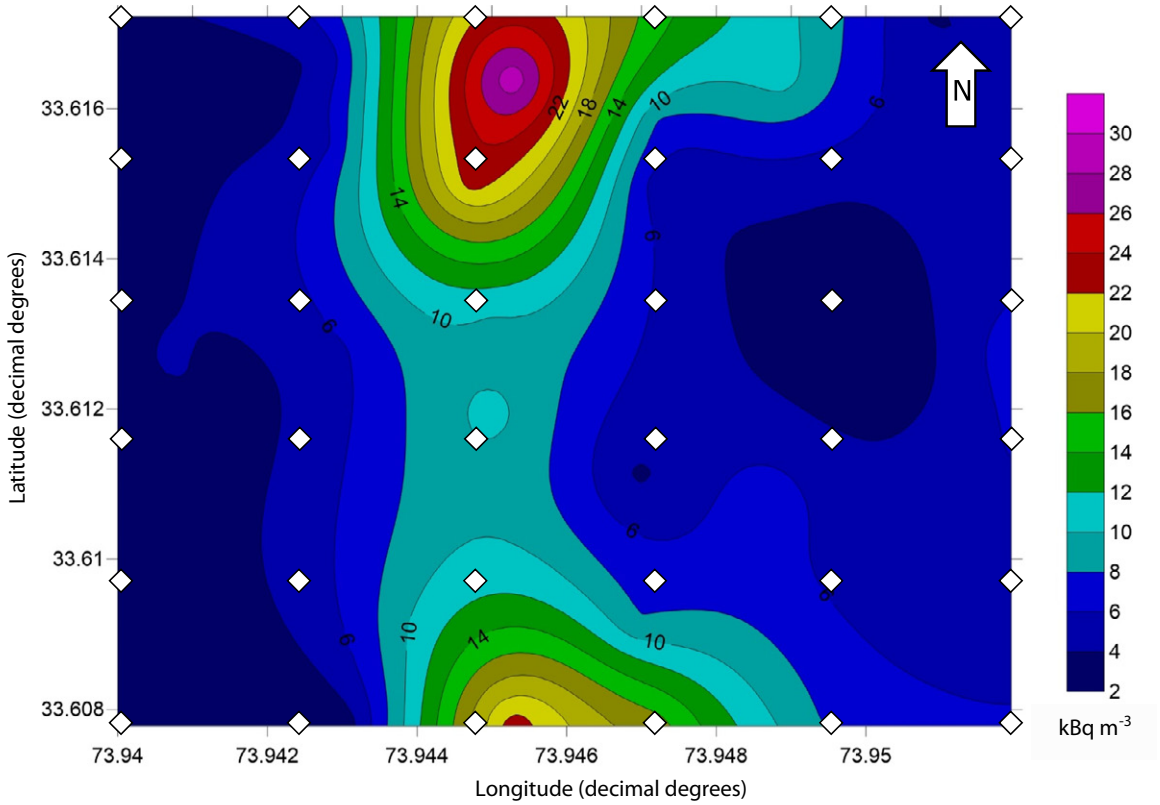

FIGURE 3. Contour map showing the spatial variability of radon concentration over the study area. The empty diamond symbols show the location of the radon sampling points.

have prominent radon concentration due to their high permeability. However, radon concentration is higher towards the shales exposed on the southwestern limb of the anticline (Fig. 4), indicating the presence of a subsurface source along the shale and carbonate contact, from which radon and other carrier gases (CO_2, CH_4, N_2 and He) are following a direct escape route.

Radon levels in the water samples were relatively low as compared to the ones in the soil. Thermal water had higher radon concentration than cold water samples. The highest concentration of radon was 9.1KBqm^{-3} for THS-6 (hot spring) and the lowest was 5.89KBqm^{-3} for river water (Table IV). Solubility of radon in water depends upon temperature, decreasing by increasing temperature (Ball *et al.*, 1991). Nevertheless, despite of its lower solubility in thermal water at higher temperature, the concentration of radon in the hot springs was higher than in the fresh water because it has been migrating to surface via thermal water.

Hydrochemistry of hot springs

The results of the physical analyses of water samples from the study area are shown in Table II. Hot spring waters were slightly acidic with pH ranging 6.62 to 6.69, and temperature ranged from 54.8ºC (THS-8) to 60.8ºC (THS-6). Flow rates were variable from one to another among hot springs, between 3.6 and 15.6Ls^{-1}. Hot springs with larger discharge showed the highest temperatures, EC and TDS values, ranging from 1115 to 1260µS/cm and 730 to 810ppm, respectively. Water samples other than hot springs were slightly alkaline with lower values of EC, TDS and temperature. Dug well and fresh water samples from cold spring had values of EC and TDS relatively higher than river samples because of their interaction with rocks. Dug well sample (TDW-1) showed abnormal values (Table II) which could be caused by thermal water recharge.

Analysis of major anions showed that the hot springs have relatively higher proportions of bicarbonate than sulphate and chloride. Ternary plot based upon concentration of major anions (Cl^-, SO_4^{-2} and HCO^{3-}) shows that the Tattapani hot springs are of bicarbonate type (Fig.5). Piper plot shows that major cations like alkali metals (Na and K) dominate the composition of the hot springs (Fig. 6). Water samples other than hot springs have relative high concentrations of Ca and Mg. Based on Piper plot, the Tattapani hot springs can be classified as Na-K-HCO_3, while the water from the open well can be classified as Ca-Mg-SO_4-Cl (Fig. 6). All other water samples are alkali bicarbonate type.

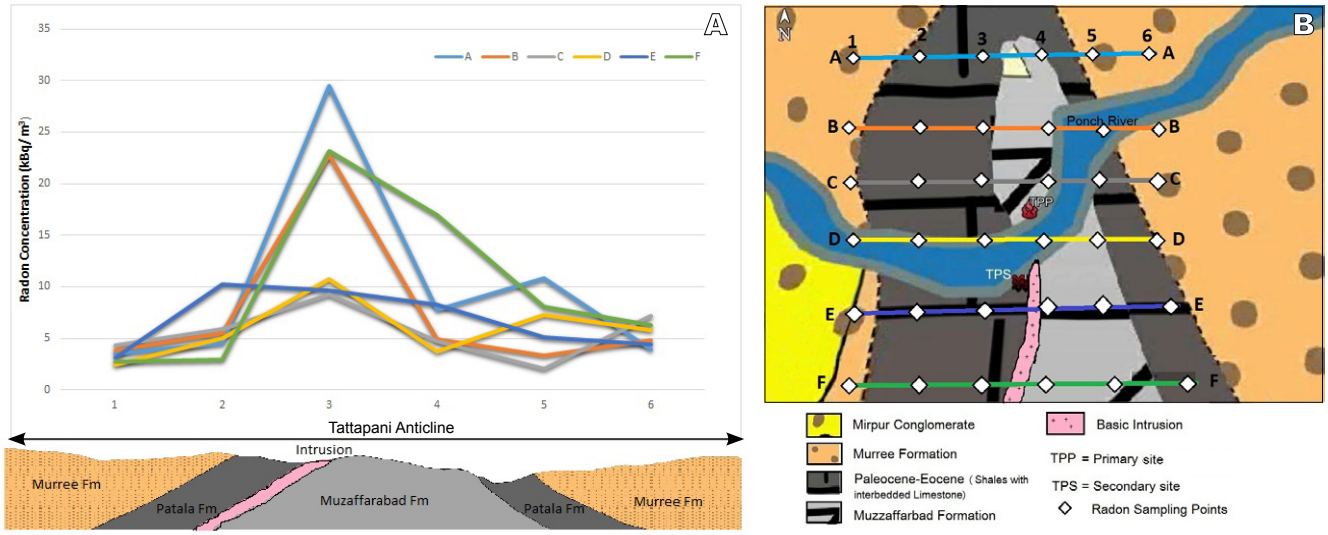

FIGURE 4. A) Variations in soil gas radon concentration along 6 traverses of grid moving across the Tattapani anticline cross-section. B) Index map showing geology as well as location of traverses A to F over Tattapani anticline.

Chemical geo-thermometry

Geo-thermometers based on total dissolved silica (*e.g.* quartz, amorphous silica and chalcedony) or on the relative concentrations of cations (*e.g.* K-Mg, Na-K, Na-K-Ca) in the thermal water can be used to calculate subsurface geothermal reservoir temperatures (Fournier, 1981). The equations of the geothermometers used in this study are as it follows:

Quartz (Truesdell, 1976)

$$T_{SiO2}(°C) = \{1315/[5.205 - \log SiO_2]\} - 273.15 \quad (2)'$$

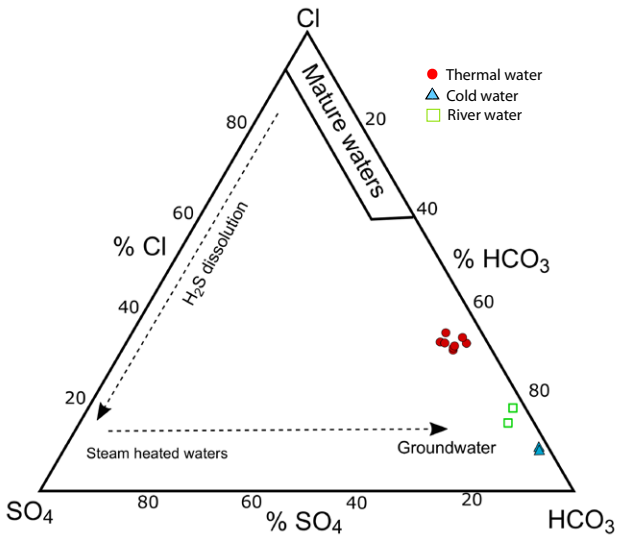

FIGURE 5. Cl-SO_4-HCO_3 ternary diagram (after Giggenbach and Goguel, 1989) showing that Tattapani hot springs are bicarbonate type.

Quartz no steam loss (Fournier, 1977)

$$T_{SiO2}(°C) = \{1309/[5.19 - \log SiO_2]\} - 273.15 \quad (3)'$$

Quartz max steam loss (Fournier, 1977)

$$T_{SiO2}(°C) = \{1522/[5.75 - \log SiO_2]\} - 273.15 \quad (4)$$

Na-K (Giggenbach, 1988)

$$T_{Na-K}(°C) = \{1390/[1.70 + \log(Na/K)]\} - 273.15 \quad (5)$$

K-Mg (Giggenbach, 1988)

$$T_{K-Mg}(°C) = \{4410/[14.0 - \log(K^2/Mg)]\} - 273.15 \quad (6)$$

K-Ca (Tonani, 1980)

$$T_{K-Ca}(°C) = \{1930/[2.92 + \log(K/Ca^{0.5})]\} - 273.15 \quad (7)'$$

Na-K-Ca-Mg (Giggenbach, 1988)

$$T_{Na-K-Ca-Mg}(°C) = \left\{16000/\left[\frac{3\log(Na/K) + 3\log(Ca/Na^2)}{3\log(Mg/Na^2) + 44.67}\right]\right\} - 273.15 \quad (8)'$$

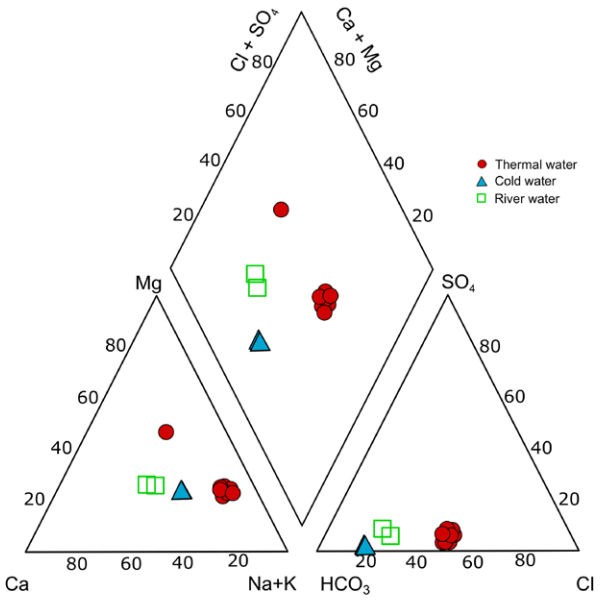

FIGURE 6. Piper plot showing the distinctive chemical nature of thermal water of Tattapani area.

Silica geo-thermometer is based on the solubility of quartz in the solution, which is highly dependent upon the temperature of fluid. According to Fournier (1989), the assumptions of silica geo-thermometer are based upon equilibrium between fluid/quartz and lack of fluid mixing during the ascending of fluid to the surface.

Reservoir temperatures based on quartz (conductive) geo-thermometer using equation (3) range between 96.01 and 122.53ºC, and between 97.54, and 120.31ºC based on quartz (adiabatic) geo-thermometer using equation (4) (Table III). The calculated reservoir temperatures suggest a near equilibrium with respect to quartz and under-saturation with respect to amorphous silica, indicating that concentration of quartz in the fluid is controlled either by adiabatic (max steam loss) or conductive (no steam loss) cooling processes.

The cation geo-thermometers assume an equilibrium state between the fluid and the minerals of the host rock. Results of the Na-K geo-thermometers using equation (5) show that the temperature ranges from 462.11 to 520.90ºC which could not be possible in this system. Such high temperatures might imply that equilibrium has not yet attained in case of Na-K exchange reactions at reservoir conditions, indicating the occurrence of dissolution of rocks (Truesdell, 1976; Fournier, 1979; Tonani, 1980; Arnórsson *et al.*, 1983; Neiva *et al.*, 1987). K-Mg requires less time than Na-K to reach equilibrium, making it more suitable for the current study. Temperatures calculated using equation (6) for K-Mg geo-thermometer, range between 111.21 and 115.16ºC (Table III). Reservoir temperatures calculated using the K-Ca geo-thermometer equation (7) are higher, ranging between 179.34 and 184.23ºC, while Na-K-Mg-Ca geo-thermometer equation (8) resulted in temperature ranging between 90.37 and 93.18ºC (Table III). Figure 7 shows a Na-K-Mg ternary diagram (Giggenbach, 1988) indicating that the thermal, cold and river waters fall into the category of immature waters. Therefore, re-equilibrium, mixing/dilution and/or dissolution of minerals associated with these cations could be the governing processes in such a system due to water-rock interaction (Reyes *et al.*, 2010), as discussed in the next section.

Subsurface processes

Waters of Tattapani hot springs show a negative correlation between δ^2H and chloride (Fig. 8A) indicating a mixing process between thermal water with low deuterium and high chloride concentration and shallow groundwater with high deuterium and low chloride concentration. Low deuterium ratio in the majority of thermal springs indicates conductive heat loss, whereas a relatively high deuterium ratio in THS-1, THS-6 and TDW-1 indicates heat loss by steam (Truesdell *et al.*, 1977). Figure 8B shows a negative correlation between $\delta^{18}O$ and chloride, while the $\delta^{18}O$ vs temperature plot (Fig. 8C) indicates mixing of ^{18}O enriched shallow groundwater with thermal water. The fact that the majority of samples lie above the trend line indicates that conductive heat loss is due to water-rock interaction (Ahmad *et al.*, 2002). Figure 9 shows an inverse relationship between tritium and electrical conductivity which also indicates that a conductive cooling process dominates over the mixing one.

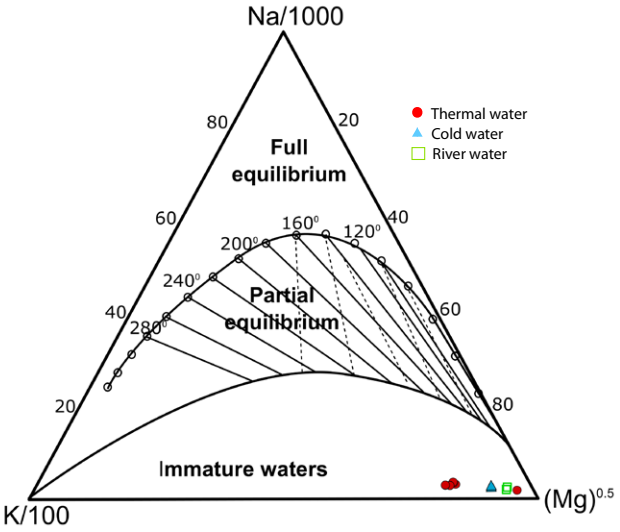

FIGURE 7. Na-K-Mg Ternary plot used to determine reservoir temperature and equilibrium between cations for geo-thermometry.

Indication of mixing is provided by plots of concentrations of tritium and chloride versus temperature (Fig. 10), and silica and sulphate concentrations as a function of chloride concentration (Fig. 11) which show a good linear relationship (Ahmad *et al.*, 2002). Tritium has a negative correlation with both the surface temperature and chloride (Fig. 10) which indicates a mixing of thermal water containing high chloride and low tritium concentration with groundwater with low chloride and high tritium concentrations. The correlation between silica and chloride concentrations (Fig. 11) suggests neither precipitation nor dissolution of quartz after mixing (Arnórsson, 1985). This hypothesis was confirmed by the absence of secondary silica precipitation around the hot springs. Figure 11 also shows a positive correlation between concentrations of sulphate and chloride, which indicates the absence of precipitation and/or dissolution of minerals containing these species during the flow of the thermal water from the reservoir up to the surface.

The extent of mixing between thermal and groundwater is calculated by assuming that the tritium concentration in the thermal waters before mixing is zero. The mixing percentage is then estimated using the following expression (Sammel and Craig, 1981; Giggenbach *et al.*, 1983; Chatterjee *et al.*, 2016):

$$X = \frac{T_{hs}}{T_{gw}} \times 100 \qquad (9)$$

where X is the percentage of the mixing, T_{hs} is the tritium concentration (in TU) of the thermal water and T_{gw} is the tritium concentration (in TU) of the local ground water. Table IV shows the concentration of tritium in the thermal, ground and river water of Tattapani area. Hot springs THS-7 and THS-8 show maximum mixing (8.68%) and THS-1, THS-5 and THS-6 show no mixing, as concentration of tritium in the latter samples was below detection limit. This indicates mixing of thermal water with different proportions of shallow groundwater before reaching the surface. Fraction of mixing can vary depending upon the season and subsurface geology of the area (Ahmad *et al.*, 2007). It is inferred from the values in Table IV that the mixing of thermal water with groundwater cannot be the only phenomenon for the thermal water cooling.

A silica concentration versus temperature diagram (Fig. 12) shows that thermal waters lie between the solubility curves of amorphous silica and quartz suggesting that thermal waters are supersaturated with respect to quartz. Quartz supersaturation in thermal waters strongly indicates conductive cooling during up flow from reservoir to the surface (Ahmed *et al.*, 2000).

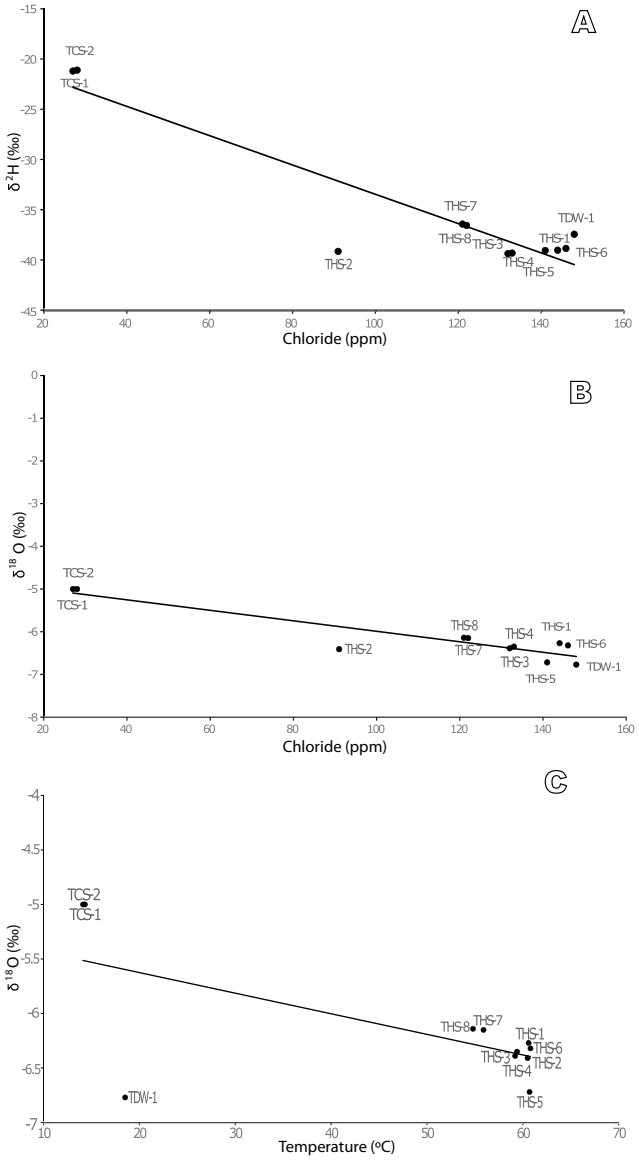

FIGURE 8. A) Relationship between chloride and δ^2H in the thermal water and shallow groundwater. B) Relationship between chloride and $\delta^{18}O$ in the thermal water and shallow groundwater. C) Relationship between temperature and $\delta^{18}O$ in the thermal water and shallow groundwater.

Conductive cooling can be estimated using the following expression (Levet *et al.*, 2006):

$$T_{adiabatic} = (1 - x)T_{rt} + x \times T_{gw} \qquad (10)$$

where $T_{adiabatic}$ is water temperature of adiabatic mixing, T_{rt} is the estimated reservoir temperature, T_{gw} is temperature of shallow groundwater and x is the percentage fraction of groundwater in thermal water. Then the extent of conductive cooling is the difference between $T_{adiabatic}$ and

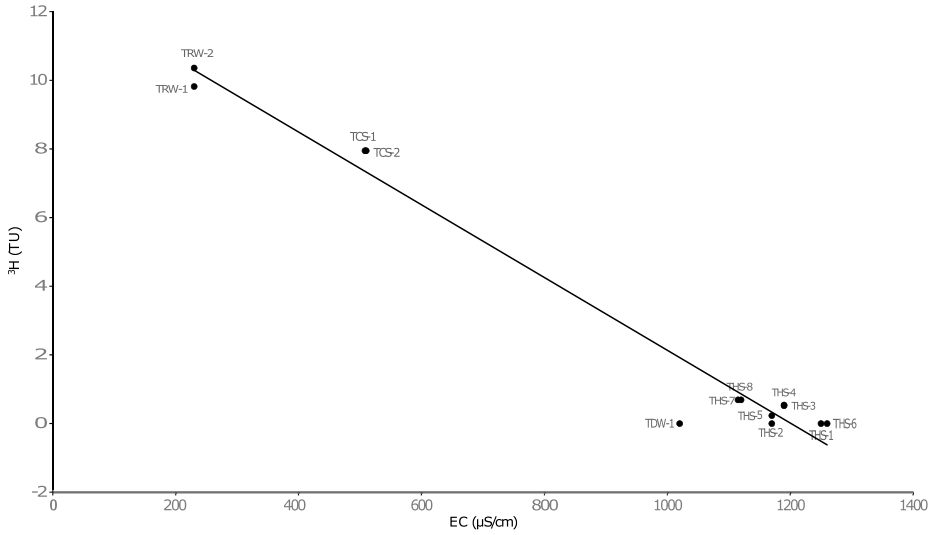

FIGURE 9. Relationship between electrical conductivity and tritium content of thermal water and shallow groundwater.

T_{hs} the measured surface temperature of the hot spring (Table IV). The results show that conductive cooling range between 33.21 and 58.9ºC, which is a significant portion of heat loss in the Tattapani hot springs. Thus, it is deduced that surface temperature of thermal water is mainly controlled by conductive cooling along with some mixing of shallow groundwater controlled by seasonal fluctuations.

Isotopic and recharge characteristics

Isotopic signatures are used to differentiate the possible origin (magmatic, oceanic and meteoric) of thermal water (Faure, 1991). $\delta^{18}O$ and $\delta^{2}H$ values of all water samples from the Tattapanihot springs lie between -6.72 to -6.14‰ and -39.37 to -36.43‰, respectively (Table IV). This isotopic data does not indicate any significant contribution of magmatic water which generally has $\delta^{18}O$ from +6 to +9‰ and $\delta^{2}H$ from -40 to -80‰ (Pearson and Rightmire, 1980; Giggenbach, 1992). Normally, ocean water has $\delta^{18}O$ and $\delta^{2}H$ about 0‰ (V-SMOW). Depleted values of $\delta^{2}H$ and $\delta^{18}O$ rule out the contribution of oceanic water. These values lie close to the Local Meteoric Water Line (LMWL) of this area (Hussain *et al.*, 1995), indicating a possible recharge from meteoric water. The $\delta^{2}H$ and $\delta^{18}O$ values of the open well water lie close to those of thermal spring water (Fig. 13), which is possibly being recharged by the seepage of deep water of hot springs. The possible source of recharge of thermal and river water could be similar (*e.g.* meteoric) due to their $\delta^{2}H$ values (Fig. 13). However, ^{18}O concentration shifts due to rock-water exchange at higher temperatures as a result of which water of hot springs seems slightly less depleted in ^{18}O (Fig. 13). The source

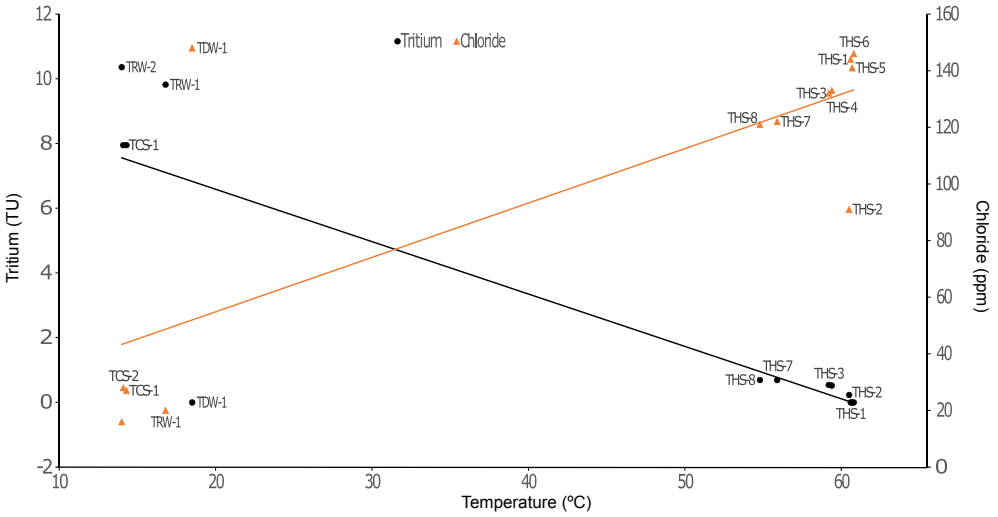

FIGURE 10. Relationship between temperature, chloride and tritium concentrations for thermal and groundwater.

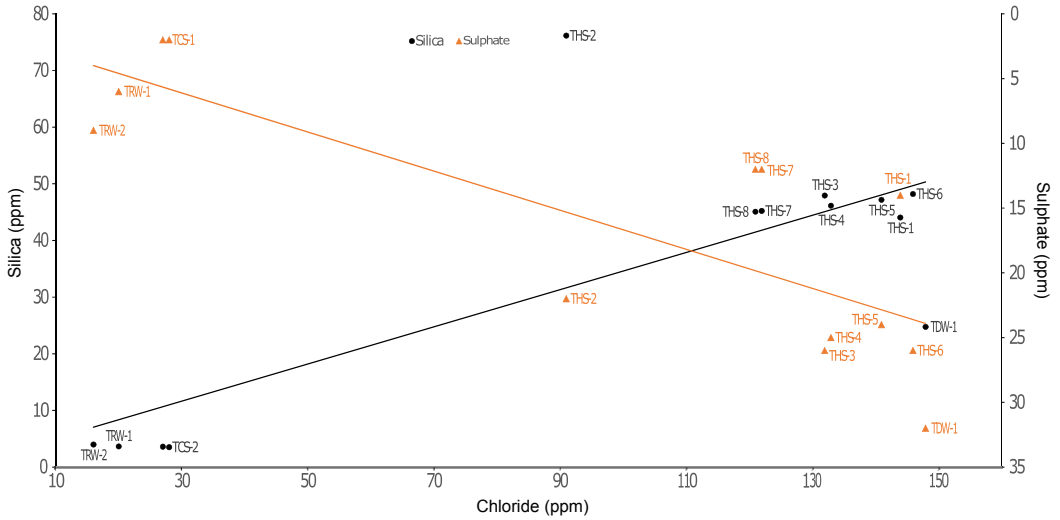

FIGURE 11. Relationship between chloride, silica and sulphate concentrations for thermal and groundwater.

of geothermal springs is probably meteoric water, feed by rain and/or snow melts from northern high altitude areas.

Tritium (^3H) with half-life of 12.4 years can be used for dating and tracing young groundwater that has been recharged within the last 50 years. Tritium content in the thermal waters of Tattapani area is found to be below detection limits (*i.e.* 0.3TU; Table IV) indicating a recharge period of more than 50 years. Tritium content in the water sample from the dug well in the area is also below detection limit, suggesting a recharge from thermal water. Instead, cold spring water has considerable tritium content (7.95TU), which indicates significant contribution of young water in the recharge. Although the H and O isotopic data indicate a meteoric water recharge, the absence (or negligible levels) of tritium in the Tattapani geothermal springs suggests an age of more than 50 years for the thermal water (Ahmad *et al.*, 2001).

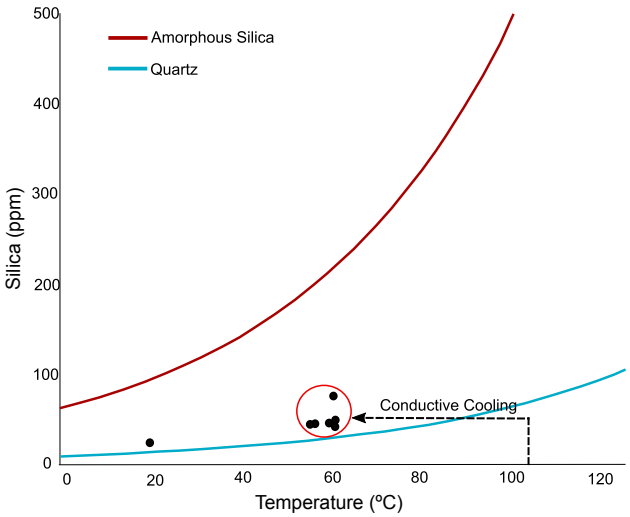

FIGURE 12. Silica concentration as a function of temperature. The plot shows heat loss of Tattapani hot springs (solid symbols) due to conductive cooling.

CONCLUSIONS

The purpose of this study was to delineate zones of high radon emissions and to evaluate hot spring waters using hydro-geochemical methods. Soil gas radon survey conducted at Tattapani area identified a zone with high radon concentration (10 to 29.5KBqm^{-3}) over the possible contact between Cambrian and Cenozoic rocks, possibly acting as a pathway for subsurface gases. Tattapani hot springs are slightly acidic with surface temperatures between 54.8 and 60.8ºC. The fluid characteristics of the Tattapani hot springs show sodium bicarbonate water type up-flow from a low temperature geothermal system with no contribution of magmatic (juvenile) water. The average reservoir temperatures are relatively low (between 101 and 115ºC) on the basis of silica and cation geo-thermometers. Plots between isotopic and chemical data show a shallow mixing of thermal water with groundwater in some of hot springs with slight dilution (~8%). Quartz solubility diagram indicates that the major heat loss is due to conductive cooling. Isotopic data of thermal waters suggest meteoric recharge (rain and/or snow-melt) from the mountains to the north of the area. The tritium content of the hot springs and shallow open well in the area is very low (below the detection limit) indicating a residence time of more than 50 years. It is concluded that the Tattapani hot springs are recharged by meteoric water, which is heated by the subsurface intrusive mass, accumulates in the Tattapani anticline

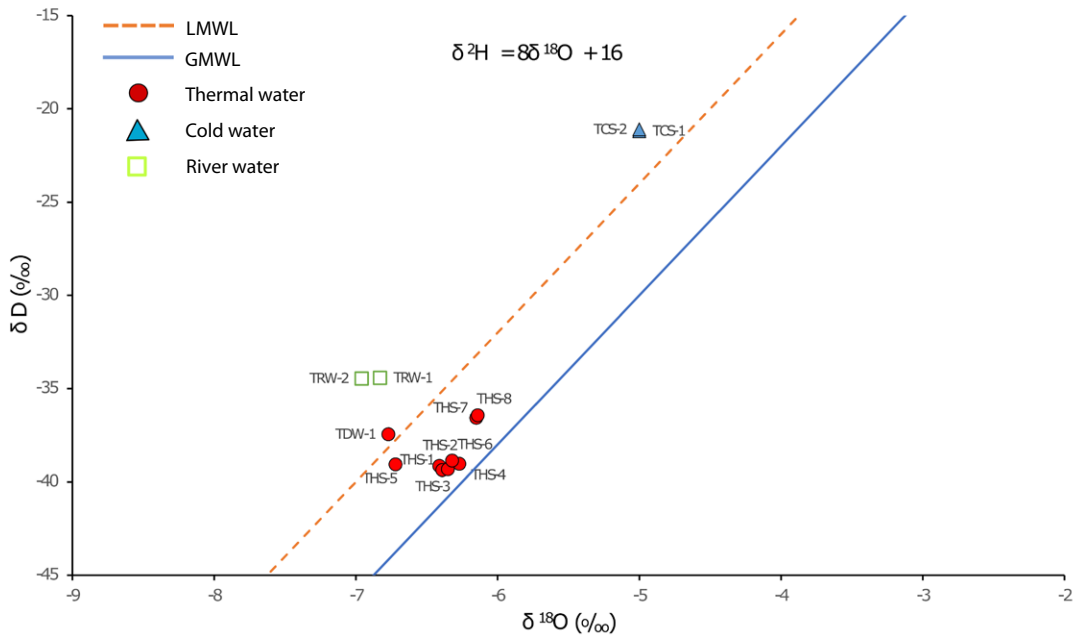

FIGURE 13. δ ²H versus δ¹⁸O plot using delta values of oxygen and hydrogen relative to LMWL (Hussain *et al.*, 1995) and GMWL (Craig, 1961).

and ultimately travels to the surface through fractured dolomitized limestones (Muzaffarabad Formation) and shales (Patala Formation).

It is recommended that the hot springs in Tattapani area, being immature and part of a low enthalpy system, may be used for direct applications (domestic: spa, fish farming, space heating, etc.). Although a magmatic heat source at depth could not have been established in previous studies, but based upon the results of the current study, an igneous source emitting radiogenic heat at depth is the most likely explanation of a geothermal system in this area. This study should be considered as preliminary and geophysical survey is recommended for detailed sub-surface understanding of the area.

ACKNOWLEDGMENTS

Authors are grateful to the Biochemistry Department (Quaid-i-Azam University, Islamabad), PINSTECH (Pakistan Institute of Nuclear Science and Technology, Islamabad) and PCRWR (Pakistan Council for Research in Water Resources, Islamabad) for providing facilities for geochemical analysis of water samples. Special thanks to Mr. Usman (Radiation Physics Lab, COMSATS Islamabad), Mr. Tahir Hussain and Mr. Emadullah Khan (Department of Geology, Abdul Wali Khan University, Mardan, Pakistan) for their valued assistance during field work. Respected reviewer is also acknowledged for his contribution in the improvement of this manuscript.

REFERENCES

Aadil, N., Rehman, T., 2013. Stratigraphy and structure of Sarda, Manil, Changpur and Naghal areas, district Kotli, Jammu and Kashmir. Journal of the Geological Society of India, 82(6), 639-648.

Ahmad, M., Tasneem, M.A., Akram, W., Hussain, S.D., Zafar, M.S., Sajjad, M.I., 2000. Isotopic investigations of Tatta Pani and Tato thermal springs: insights to their origin, age and subsurface history. Nuclear Science Journal of Malaysia (JSNM), 18(2), 95-99.

Ahmad, M., Akram, W., Hussain, S.D., Sajjad, M.I., Zafar, M.S., 2001. Origin and subsurface history of geothermal water of Murtazabad area, Pakistan-isotopic evidence. Applied Radiation and Isotopes, 55(5), 731-736.

Ahmad, M., Akram, W., Ahmad, N., Tasneem, M.A., Rafiq, M., Latif, Z., 2002. Assessment of reservoir temperatures of thermal springs of the northern areas of Pakistan by chemical and isotope geothermometry. Geothermics, 31(5), 613-631.

Ahmad, M., Sheikh, M.R., Akram, W., Tasneem, M.A., Iqbal, N., Latif, Z., 2007. Investigation of geothermal fields in Himalayan range in Pakistan using isotope and chemical techniques. Pakistan Institute of Nuclear Science and Technology, Islamabad (Pakistan). Isotope Application Division, Report PINSTECH/RIAD-202, 32pp.

APHA (American Public Health Association), 2005. Standard Methods for the Examination of Water and Wastewater. 21st ed. American Public Health Association, Washington DC, 1220p.

Arnórsson, S., Gunnlaugsson, E., Svavarsson, H., 1983. The chemistry of geothermal waters in Iceland. III. Chemical

geothermometry in geothermal investigations. Geochimica et Cosmochimica Acta, 47(3), 567-577.

Arnórsson, S., 1985. The use of mixing models and chemical geothermometers for estimating underground temperatures in geothermal systems. Journal of Volcanology and Geothermal Research, 23(3-4), 299-335.

Arnórsson, S., 2000. Isotopic and chemical techniques in geothermal exploration, development and use. International Atomic Energy Agency, 109-111.

Ashraf, M., Chaudhry, M.N., Qureshi, K.A., 1983. Stratigraphy of Kotli area of Azad Kashmir and its correlation with standard type areas of Pakistan. Kashmir Journal of Geology, 1(1), 19-30.

Ashraf, M., Chaudhry, M.N., Malik, R.H., 1986. Bituminous/ anthracitic coal of Kotli District, Azad Kashmir. Kashmir Journal of Geology, 4, 1-14.

Bakht, M.S., 2000. An Overview of Geothermal Resources of Pakistan. Kyushu-Tohoku (Japan), Proceedings of the World Geothermal Congress, 77-83.

Balcazar, M., Gonzalez, E., Ortega, M., Flores, J.H., 1993. Geothermal energy prospecting in El Salvador. Nuclear Tracks and Radiation Measurements, 22(1), 273-276.

Ball, T.K., Cameron, D.G., Colman, T.B., Roberts, P.D., 1991. Behaviour of radon in the geological environment: a review. Quarterly Journal of Engineering Geology and Hydrogeology, 24(2), 169-182.

Chatterjee, S., Sharma, S., Ansari, M.A., Deodhar, A.S., Low, U., Sinha, U.K., Dash, A., 2016. Characterization of subsurface processes and estimation of reservoir temperature in Tural and Rajwadi geothermal fields, Maharashtra, India. Geothermics, 59, 77-89.

Craig, H., 1961. Isotopic variations in meteoric waters. Science, 133(3465), 1702-1703.

Epstein, S., Mayeda, T., 1953. Variation of O^{18} content of waters from natural sources. Geochimica et Cosmochimica Acta, 4(5), 213-224.

Faure, G., 1991. Principles and applications of inorganic geochemistry: a comprehensive textbook for geology students. USA, Macmillan Publishing Company, 626pp.

Fleischer, R.L., 1988. Radon in the environment-opportunities and hazards. Nuclear Tracks and Radiation Measurements, 14, 421-435.

Fournier, R.O., 1977. Chemical geothermometers and mixing models for geothermal systems. Geothermics, 5(1), 41-50.

Fournier, R.O., 1979. Geochemical and hydrologic considerations and the use of enthalpy-chloride diagrams in the prediction of underground conditions in hot-spring systems. Journal of Volcanology and Geothermal Research, 5(1), 1-16.

Fournier, R.O., 1981. Application of water geochemistry to geothermal exploration and reservoir engineering. In: Ryback, L., Muffler, L.J.P. (eds.). Geothermal Systems: Principles and Case Histories. New York, Wiley, 109-143.

Fournier, R.O., 1989. Lectures on geochemical interpretation of hydrothermal waters (No. 10). United Nations University Geothermal Training Programme, Iceland, Report 10, 73pp.

Mureed, S., Majeed, A., Malik, A.H., Ahmed, M., Mughal, M.N., Khan, R., Hussain, A., 2004. Geological map of Kotli area, Parts of Kotli and Sudhnoti Districts, AJK. Geological Survey of Pakistan Map Series. Vol. 6, 23, sheet no. 43 G/14. scale 1:50,000.

Giggenbach, W.F., 1988. Geothermal solute equilibria, derivation of Na-K-Mg-Ca geoindicators. Geochimica et Cosmochimica Acta, 52(12), 2749-2765.

Giggenbach, W.F., 1992. Isotopic shifts in waters from geothermal and volcanic systems along convergent plate boundaries and their origin. Earth and planetary science letters, 113(4), 495-510.

Giggenbach, W.F., Goguel, R.T., 1988. Methods for the collection and analysis of geothermal and volcanic water and gas samples. New Zealand, Department of Scientific and Industrial Research, Report, CD 2387, 53pp.

Giggenbach, W.F., Goguel, R.L., 1989. Collection and analysis of geothermal and volcanic water and gas discharges. Petone (New Zealand), Department of Scientific and Industrial Research (DSIR), Chemistry Division, Report No.: CD 2401, 4th Edition, 88pp.

Giggenbach, W.F., Gonfiantini, R., Jangi, B.L., Truesdell, A.H., 1983. Isotopic and chemical composition of Parbati valley geothermal discharges, north-west Himalaya, India. Geothermics, 12(2-3), 199-222.

Gingrich, J.E., 1984. Radon as a geochemical exploration tool. Journal of Geochemical Exploration, 21(1), 19-39.

Haerudin, N., Munadi, S., Suryanto, W., 2013. A Soil Gas Radon Survey to Determine Fault at Southern Part of Rajabasa Geothermal Field, Lampung Indonesia. International Journal of Engineering and Technology, 13(1), 75-81.

Hussain, S.D., Asghar, G., 1982. Programme for TI Programmable Calculator for Calculation of ^{3}H Concentration of Water Samples. Islamabad (Pakistan), Institute of Nuclear Science and Technology, Isotope Application Division, Report PINSTECH/RIAD-102, 45pp.

Hussain, S.D., Ahmad, M., Gonfiantini, R., Akram, W., Sajjad, M.I., Tasneem, M.A., 1995. Isotopic and chemical studies of geothermal waters of Northern Areas of Pakistan (Report IAEA-TECDOC-788). International Atomic Energy Agency (IAEA), Vienna (Austria), 127-147.

Hussain, A., Yeats, R.S., Lisa, M., 2009. Geological setting of the 8 October 2005 Kashmir earthquake. Journal of seismology, 13(3), 315-325.

Levet, S., Berger, G., Munoz, M., Toutain, J. P., 2006. A new and fast method to determine mixing and conductive cooling of thermal waters in carbonate-evaporite environments. Geothermics, 35(3), 285-301.

López, A., Gutiérrez, L., Razo, A., Balcázar, M., 1987. Radon mapping for locating geothermal energy sources. Nuclear Instruments and Methods in Physics Research Section A: Accelerators, Spectrometers, Detectors and Associated Equipment, 255(1), 426-429.

Lund, J.W., Freeston, D.H., Boyd, T.L., 2005. Direct application of geothermal energy: 2005 worldwide review. Geothermics, 34(6), 691-727.

Mogro-Campero, A., Fleischer, R.L., 1977. Subterrestrial fluid convection: a hypothesis for long-distance migration of radon within the earth. Earth and Planetary Science Letters, 34(2), 321-325.

Morawska, L., Phillips, C.R., 1993. Dependence of the radon emanation coefficient on radium distribution and internal structure of the material. Geochimica et Cosmochimica Acta, 57(8), 1783-1797.

Munir, M.U.H., Baig, M.S., 2006. Paleogene biostratigraphy of Tattapani, Kotli Azad Kashmir, Northwest sub-Himalayas, Pakistan. Journal of Himalayan Earth Sciences, 39, 39-48.

Neiva, A.M., Neiva, J.M., Parry, S.J., 1987. Geochemistry of the granitic rocks and their minerals from Serra da Estrela, Central Portugal. Geochimica et Cosmochimica Acta, 51(3), 439-454.

Nishimura, S., Katsura, I., 1990. Radon in soil gas: Applications in exploration and earthquake prediction. In: Durrance, E.M. (Ed.), Geochemistry of Gaseous Elements and Compounds. The Ophrastus Publication, S.A. Athens, pp. 497–533.

Pearson, F.J., Rightmire, C.T., 1980. Sulphur and oxygen isotopes in aqueous sulphur compounds. Handbook of environmental isotope geochemistry, 1, 227-258.

Phuong, N. K., Harijoko, A., Itoi, R., Unoki, Y., 2012. Water geochemistry and soil gas survey at Ungaran geothermal field, central Java, Indonesia. Journal of Volcanology and Geothermal Research, 229, 23-33.

Reyes, A.G., Christenson, B.W., Faure, K., 2010. Sources of solutes and heat in low-enthalpy mineral waters and their relation to tectonic setting, New Zealand. Journal of Volcanology and Geothermal Research, 192(3), 117-141.

Sac, M.M., Harmansah, C., Camgoz, B., Sozbilir, H., 2011. Radon monitoring as the earthquake precursor in fault line in Western Turkey. Ekoloji, 20(79), 93-98.

Sammel, E.A., Craig, R.W., 1981. The geothermal hydrology of Warner Valley, Oregon: a reconnaissance study. Reston, (Virginia, USA), Geological Survey (USGS), Professional Paper 1044-I, 147pp.

Shuja, T.A., 1986. Geothermal areas in Pakistan. Geothermics, 15(5), 719-723.

Thakur, V.C., Jayangondaperumal, R., Malik, M.A., 2010. Redefining Medlicott–Wadia's main boundary fault from Jhelum to Yamuna: An active fault strand of the main boundary thrust in northwest Himalaya. Tectonophysics, 489(1), 29-42.

Todaka, N., Shuja, T.A., Jamiluddin, S., Khan, N.A., Pasha, M.A., Iqbal, M., 1988. A preliminary study for geothermal development project in Pakistan. Geological Survey of Pakistan Memoirs, 107, 4-47.

Tonani, F.B., 1980. Some remarks on the application of geochemical techniques in geothermal exploration. In: Strub, A.S., Ungemach, P. (eds.). Advances in European Geothermal Research. The Netherlands, Springer, 428-443.

Toutain, J.P., Baubron, J.C., 1999. Gas geochemistry and seismotectonics: a review. Tectonophysics, 304(1), 1-27.

Truesdell, A.H., 1976. Summary of Section III-Geochemical techniques in exploration. Proceedings: 2nd United Nations Symposium on the Development and Use of Geothermal Resources. San Francisco, California, 20-29 May, 1975, vol. 1, 53-79.

Truesdell, A.H., Nathenson, M., Rye, R.O., 1977. The effects of subsurface boiling and dilution on the isotopic compositions of Yellowstone thermal waters. Journal of Geophysical Research, 82(26), 3694-3704.

Wadia, D.N., 1928. The geology of Poonch state (Kashmir) and adjacent parts of the Panjab. India, Memoirs of Geological Survey of India, 51, 257-268.

Watson, J.C., 1978. Sampling and analysis methods for geothermal fluids and gases (No. PNL-MA-572). Battelle Pacific Northwest Labs., Richland, WA (USA), 399pp.

Wells, N.A., Gingerich, P.D., 1987. Paleoenvironmental interpretation of Paleogene strata near Kotli, Azad Kashmir, Northeastern Pakistan. Kashmir Journal of Geology, 5, 23-41.

Whitehead, N.E., 1984. Geothermal prospecting by ground radon measurements. Journal of Volcanology and Geothermal esearch, 20(3), 213-229.

Zaigham, N.A., Nayyar, Z.A., Hisamuddin, N., 2009. Review of geothermal energy resources in Pakistan. Renewable and Sustainable Energy Reviews, 13(1), 223-232.

Manuscript received January 2017;
revision accepted April 2017;
published Online July 2017.

APPENDIX I

TABLE I. Radon concentration measured at 36 sample locations around hot springs along with exposed geology at each point. Distribution of soil gas into three populations (low, high and anomalous) using statistical analysis, *i.e.* Mean (average) and Standard deviation (difference from the mean)

Sr. No	Location Code	Geographic Coordinates (Degree, min, sec)		Mean Radon Concentration (KBq m^{-3})	Lithology
1	A1	33°37'0.58"N	73°56'26.65"E	3.50	Sandstone (Murree Fm)
2	A2	33°37'0.60"N	73°56'34.42"E	4.50	Shale (Eocene-Murree Contact)
3	A3	33°37'0.59"N	73°56'42.19"E	29.50	Shale (PatalaFm)
4	A4	33°37'0.58"N	73°56'49.93"E	7.80	Thick Soil
5	A5	33°37'0.59"N	73°56'57.73"E	10.80	Soil cover
6	A6	33°37'0.62"N	73°57'5.42"E	3.92	Sandstone (Murree Fm)
7	B1	33°36'54.09"N	73°56'26.68"E	3.80	Murree Fm
8	B2	33°36'54.10"N	73°56'34.42"E	5.50	Limestone (MargallaFm)
9	B3	33°36'54.07"N	73°56'42.16"E	22.80	Soil
10	B4	33°36'54.11"N	73°56'49.92"E	4.87	Soil
11	B5	33°36'54.12"N	73°56'57.67"E	3.29	Loose Gravel (Fluvial)
12	B6	33°36'54.11"N	73°57'5.39"E	4.80	Sandstone (Murree Fm)
13	C1	33°36'47.65"N	73°56'26.64"E	4.29	Soil
14	C2	33°36'47.64"N	73°56'34.40"E	5.90	Soil
15	C3	33°36'47.65"N	73°56'42.16"E	9.30	Soil
16	C4	33°36'47.64"N	73°56'49.96"E	4.70	Limestone (Muzaffarabad Fm)
17	C5	33°36'47.63"N	73°56'57.70"E	2.05	Gravel (River Deposits)
18	C6	33°36'47.62"N	73°57'5.43"E	7.20	Fertile Soil
19	D1	33°36'41.16"N	73°56'26.64"E	2.40	Loose Gravel
20	D2	33°36'41.15"N	73°56'34.39"E	5.02	Loose Gravel
21	D3	33°36'41.14"N	73°56'42.17"E	10.70	Loose Gravel
22	D4	33°36'41.13"N	73°56'49.90"E	3.72	Limestone (Muzaffarabad Fm)
23	D5	33°36'41.14"N	73°56'57.63"E	7.30	Limestone (Muzaffarabad Fm)
24	D6	33°36'41.13"N	73°57'5.41"E	5.80	Loamy Soil
25	E1	33°36'34.68"N	73°56'26.65"E	3.10	Regolith (Murree Fm)
26	E2	33°36'34.66"N	73°56'34.39"E	10.20	Soil
27	E3	33°36'34.67"N	73°56'42.14"E	9.60	Loose Shale (PatalaFm)
28	E4	33°36'34.67"N	73°56'49.93"E	8.23	Loose Shale (PatalaFm)
29	E5	33°36'34.68"N	73°56'57.68"E	5.14	Shale (PatalaFm)
30	E6	33°36'34.69"N	73°57'5.43"E	4.41	Shale (PatalaFm)
31	F1	33°36'28.21"N	73°56'26.65"E	2.70	Young Soil (Murree Fm)
32	F2	33°36'28.17"N	73°56'34.41"E	2.95	Young Soil (Murree Fm)
33	F3	33°36'28.17"N	73°56'42.16"E	23.2	Shale + Soil
34	F4	33°36'28.19"N	73°56'49.93"E	16.9	Stream Deposits
35	F5	33°36'28.20"N	73°56'57.64"E	8.07	Shale (PatalaFm)
36	F6	33°36'28.19"N	73°57'5.43"E	6.32	

Mean (m)	7.62
Standard deviation SD (σ)	6.23
Low (concentration<σ)	< 6.23
High (σ<concentration<σ+m)	6.23 – 13.84
Anomalous (σ+m<concentration<σ+2*m)	13.84 –21.46

TABLE II. Physical properties and chemical composition of water samples collected from the Tattapani area

Sr. No.	Location Code	Geographic Coordinates	Flow Rate (L/s)	Temperature (°C)	pH	EC (µS/cm)	TDS (ppm)	Ca	Mg	Na	K	HCO_3	Cl	SO_4	SiO_2
								ppm							
1	THS-1	33°36'43.57"N 73°56'49.35"E	11.8	60.6	6.62	1250	800	30.93	40.38	153.97	111.42	262	144	14	44.07
2	THS-2	33°36'43.32"N 73°56'49.56"E	4.3	60.5	6.62	1170	790	34.45	41.10	133.67	121.76	152	91	22	76.17
3	THS-3	33°36'42.90"N 73°56'49.41"E	7.2	59.2	6.62	1190	800	33.74	41.37	129.11	126.32	242	132	26	47.94
4	THS-4	33°36'43.10"N 73°56'50.16"E	6.8	59.4	6.62	1190	795	33.21	41.56	127.78	127.63	241	133	25	46.14
5	THS-5	33°36'43.88"N 73°56'49.52"E	9.1	60.7	6.65	1170	790	31.30	42.72	151.48	113.14	222	141	24	47.19
6	THS-6	33°36'43.38"N 73°56'49.24"E	15.6	60.8	6.62	1260	810	30.57	42.23	149.26	112.47	265	146	26	48.21
7	THS-7	33°36'37.03"N 73°56'45.50"E	3.6	55.9	6.69	1120	740	35.21	39.12	120.34	118.31	210	122	12	45.23
8	THS-8	33°36'36.91"N 73°56'45.56"E	2.5	54.8	6.69	1115	730	34.11	38.92	120.14	118.11	208	121	12	45.08
9	TDW-1	33°36'46.20"N 73°56'46.61"E	-	18.5	7.44	1020	690	35.98	43.97	42.24	20.33	252	148	32	24.76
10	TCS-1	33°36'34.64"N 73°56'46.09"E	4.3	14.3	7.43	508	338	37.85	19.43	49.95	36.46	198	27	2	3.61
11	TCS-2	33°36'34.64"N 73°56'46.39"E	5.7	14.1	7.45	510	340	38.42	19.81	51.19	36.85	202	28	2	3.52
12	TRW-1	33°36'42.75"N 73°56'51.62"E	-	16.8	7.66	230	160	34.78	13.51	20.62	19.65	92	20	6	3.65
13	TRW-2	33°36'39.22"N 73°56'45.65"E	-	14	7.63	230	160	35.16	14.44	28.20	18.90	92	16	9	3.99

THS = Hot Spring, TDW = Dug Well, TCS = Cold(fresh) water, TRW = River Water

TABLE III. Estimated reservoir temperatures of Tattapani hot springs using different silica and cation geo-thermometers

Sample ID	Surface Temperature (°C)	Estimated Reservoir Temperature (°C)						
		Quartz (Truesdell, 1976)	Quartz no steam (Fournier, 1977)	Quartz max steam (Fournier, 1977)	Na-K (Giggenbach, 1988)	K-Mg (Giggenbach, 1988)	K-Ca (Tonani, 1980)	Na-K-Ca-Mg (Giggenbach, 1988)
THS-1	60.6	96.14	96.01	97.54	462.11	111.59	184.01	90.37
THS-2	60.5	122.55	122.53	120.31	503.15	113.93	182.37	92.06
THS-3	59.2	99.97	99.86	100.87	516.84	114.93	180.18	92.88
THS-4	59.4	98.22	98.10	99.35	520.90	115.16	179.34	93.18
THS-5	60.7	99.25	99.13	100.24	467.49	111.22	183.56	90.82
THS-6	60.8	100.23	100.12	101.09	469.01	111.21	183.29	90.95
THS-7	55.9	97.32	97.19	98.56	517.80	113.82	184.23	92.35
THS-8	54.8	97.17	97.04	98.43	517.79	113.84	183.56	92.49

Geologica Acta, 15(3), 217-230, I-III (2017)
DOI: 10.1344/GeologicaActa2017.15.3.5

TABLE IV. Environmental isotope values and extent of conductive cooling

Sample ID	Rn^{222} KBq m^{-3}	^{18}O (‰)	^{2}H (‰)	^{3}H (TU)	±1σ	Fraction of cold water component (x) (%)	(T_{spring})(◦C)	($T_{adiabatic}$)(◦C)	Extent of conductive cooling ($T_{adiabatic}$-T_{spring})(◦C)
THS-1	8.28	-6.27	-39.04	0	0.2	0.00	60.6	96.01	35.41
THS-2	7	-6.41	-39.15	0.23	0.3	2.89	60.5	119.40	58.90
THS-3	7.86	-6.39	-39.37	0.54	0.2	6.79	59.2	94.04	34.84
THS-4	8.12	-6.35	-39.32	0.52	0.2	6.54	59.4	92.61	33.21
THS-5	8.42	-6.72	-39.07	0	0.2	0.00	60.7	99.13	38.43
THS-6	9.1	-6.32	-38.86	0	0.2	0.00	60.8	100.12	39.32
THS-7	6.97	-6.15	-36.57	0.69	0.3	8.68	55.9	89.99	34.09
THS-8	6.96	-6.14	-36.43	0.69	0.3	8.68	54.8	89.85	35.05
TDW-1	6.9	-6.77	-37.45	0	0.3	0.00	18.5	71.66	53.16
TCS-1	6.31	-5	-21.2	7.95	0.5	-	14.3	-	-
TCS-2	6.32	-5	-21.1	7.95	0.5	-	14.1	-	-
TRW-1	5.89	-6.83	-34.42	9.82	0.6	-	16.8	-	-
TRW-2	5.93	-6.96	-34.46	10.36	0.6	-	14	-	-

THS: Hot Spring, TDW: Dug Well, TCS: Cold(fresh) water, TRW: River Water